fluids

MDPI

Article

# Heat Transfer and Pressure Drop in Fully Developed Turbulent Flows of Graphene Nanoplatelets–Silver/Water Nanofluids

**Mohammad Reza Safaei [1], Goodarz Ahmadi [2,*], Mohammad Shahab Goodarzi [3], Mostafa Safdari Shadloo [4], Hamid Reza Goshayeshi [3] and Mahidzal Dahari [5]**

1 Department of Mechanical Engineering, Faculty of Engineering, University of Malaya, Kuala Lumpur 50603, Malaysia; cfd_safaei@um.edu.my
2 Department of Mechanical and Aeronautical Engineering, Clarkson University, Potsdam, NY 13699-5700, USA
3 Department of Mechanical Engineering, Mashhad Branch, Islamic Azad University, Mashhad 918714757, Iran; shahabg25269@yahoo.com (M.S.G.); Goshayshi@yahoo.com (H.R.G.)
4 CORIA-UMR 6614, Normandie University, CNRS-University & INSA of Rouen, St Etienne du Rouvray 76800, France; mostafa.safdari-shadloo@insa-rouen.fr
5 Department of Electrical Engineering, Faculty of Engineering, University of Malaya, Kuala Lumpur 50603, Malaysia; mahidzal@um.edu.my
* Correspondence: gahmadi@clarkson.edu; Tel.: +1-315-268-2322

Academic Editors: Phuoc X. Tran and Mehrdad Massoudi
Received: 16 March 2016; Accepted: 24 June 2016; Published: 29 June 2016

**Abstract:** This study examined the heat transfer coefficient, friction loss, pressure drop and pumping power needed for the use of nanofluid coolants made of a mixture of suspension of graphene nanoplatelets–silver in water in a rectangular duct. A series of calculations were performed for the coolant volume flow rate in the range of $5000 \leqslant Re \leqslant 15{,}000$ under a fully developed turbulent flow regime and different nanosheet concentrations up to 0.1 weight percent. The thermo-physical properties of the nanofluids were extracted from the recent experimental work of Yarmand et al. (Graphene nanoplatelets-silver hybrid nanofluids for enhanced heat transfer. *Energy Convers. Manag.* 2015, *100*, 419–428). The presented results indicated that the heat transfer characteristics of the nanofluid coolants improved with the increase in nanosheet concentration as well as the increase in the coolant Reynolds number. However, there was a penalty in the duct pressure drop and an increase in the required pumping power. In summary, the closed conduit heat transfer performance can be improved with the use of appropriate nanofluids based on graphene nanoplatelets–silver/water as a working fluid.

**Keywords:** graphene nanoplatelets-silver nanosheet; heat transfer; pressure drop; rectangular duct

**PACS:** 47.61.-k; 40; 61.46.Fg

## 1. Introduction

Heat exchangers are widely used in industries to effectively transfer thermal energy from one medium to another. They are typically classified according to the flow arrangement and the type of heat exchanger construction. The focus of the present study is the non-circular cross-section's plate heat exchangers which are used extensively in various applications including in power generation and power recovery, the food industry, the chemical industry, refrigeration and air conditioning systems [1]. The compact design and the high energy efficiency of the plate heat exchangers have made them quite attractive [2]. Plain and corrugated plate heat exchangers with non-circular cross-sections have shown

superior performance compared to other conventionally used heat exchangers such as concentric or double-pipe heat exchangers. This is due to the larger available surface area for transporting the heat with the same volumetric capacity [3].

In addition to the physical design of heat exchangers, the thermal properties of heat transfer (working) fluid flowing through the heat exchangers play a crucial role in the overall energy efficiency of the system [4]. Choi and Eastman [5] introduced the concept of dispersing the nanoparticles in base fluids to form nanofluids as an enhanced working fluid. While the potential usage of liquid-solid mixtures to enhance thermal performance has been around, the utilization of nanometer-size particles in nanofluids ensures a more stable fluid that would also diminish the potential for erosion, corrosion, fouling and pipe blockage which could occur when large particles are used [6].

After the successful demonstration of the superior thermal performance of nanofluid by Choi and Eastman [5], many other researchers investigated the formation and characterization of nanofluids [7,8]. In particular, several studies were performed on the application of nanofluids in various heat exchangers [9,10].

The turbulent flow of water-based nanofluids in a corrugated plate heat exchanger was explored by Pandey and Nema [11] using the aluminum oxide nanoparticles. For transferring the same amount of thermal energy, they reported a lower required flow rate for the nanofluid compared to water, while the pressure drop was higher for the nanofluid.

There has been some controversy on the thermal enhancement of CuO/water nanofluids. Taws et al. [12] experimentally examined the performance of CuO/water nanofluids in a chevron-type two-channel plate heat exchanger for low-Reynolds-number flows with $Re < 1000$. They reported no noticeable increase in the Nusselt number for the CuO/water nanofluid with 2.00 vol. % concentration, and a decrease in the heat transfer rate when the volume fraction of CuO was 4.65%. For the same condition, however, Elias et al. [13] reported a substantial increase in the heat transfer enhancement of the CuO/water nanofluid when a solid concentration of only 1.5 vol. % was used.

The presented literature survey with the noted inconsistency in some cases suggests the need for additional research on nanofluids as high performance working fluids for heat exchangers [14,15]. In particular, further investigation is required to fill the existing gap for the non-circular closed-channel flow. Therefore, in this paper, a numerical study is performed to investigate the heat transfer coefficient, pressure drop, friction factor, and needed pumping power for graphene nanoplatelets-silver (GNP-silver) water-based nanofluid at various solid volume fractions flowing through a rectangular duct. The results from the present study may find applications for a high performance coolant in corrugated plate heat exchangers [16], solar collectors and electronic devices [17].

## 2. Nanofluid Properties

The exact evaluation of nanofluid properties is essential for the accuracy of the computation modeling effort. Here, the thermo-physical properties of nanofluids are extracted from the recent measurements of Yarmand et al. [18] and are presented in Table 1.

**Table 1.** Thermo-physical properties of the base fluid and nanofluids [18].

| Thermophysical Properties | Weight Percentage | 20 °C | 25 °C | 30 °C | 35 °C | 40 °C |
|---|---|---|---|---|---|---|
| Density (Kg/m$^3$) | $\phi$ = 0.00% | 997.91 | 996.68 | 995.29 | 993.68 | 991.99 |
| | $\phi$ = 0.06% | 998.5 | 997.40 | 996.01 | 994.45 | 992.53 |
| | $\phi$ = 0.10% | 998.90 | 997.80 | 996.30 | 994.67 | 992.93 |
| Thermal Conductivity (W/m· K) | $\phi$ = 0.00% | 0.59 | 0.60 | 0.61 | 0.62 | 0.63 |
| | $\phi$ = 0.06% | 0.64 | 0.64 | 0.65 | 0.67 | 0.72 |
| | $\phi$ = 0.10% | 0.69 | 0.70 | 0.72 | 0.74 | 0.77 |
| Viscosity (Pa· s) | $\phi$ = 0.00% | $1.1 \times 10^{-3}$ | $9.7 \times 10^{-4}$ | $8.6 \times 10^{-4}$ | $7.9 \times 10^{-4}$ | $7.1 \times 10^{-4}$ |
| | $\phi$ = 0.06% | $1.20 \times 10^{-3}$ | $1.07 \times 10^{-3}$ | $9.6 \times 10^{-4}$ | $9.1 \times 10^{-4}$ | $8.4 \times 10^{-4}$ |
| | $\phi$ = 0.10% | $1.27 \times 10^{-3}$ | $1.13 \times 10^{-3}$ | $1.03 \times 10^{-3}$ | $9.8 \times 10^{-4}$ | $9.2 \times 10^{-4}$ |

In the present study, regressions of the experimental data were performed and empirical equations for the effective viscosity and thermal conductivity of the nanofluid were obtained. Accordingly, for 0.0 wt. % $\leqslant \phi \leqslant$ 0.1 wt. % and 20 °C $\leqslant T \leqslant$ 40 °C,

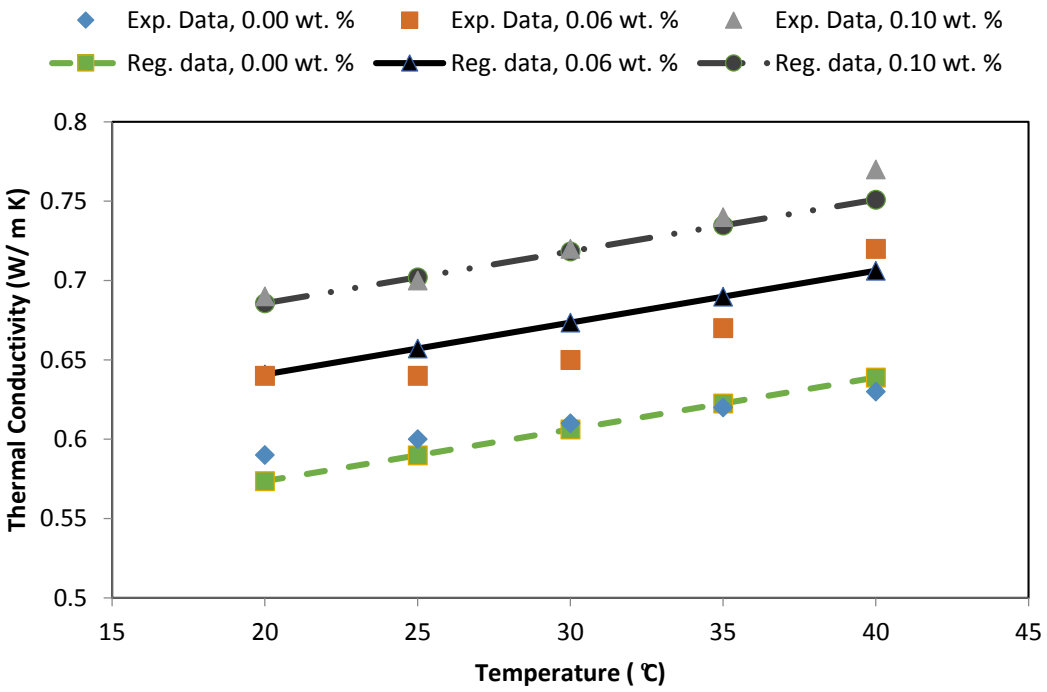
$$\mu = 0.001425 + (0.001803\varphi) + \left(-1.80 \times 10^{-5} T\right) \quad (1)$$

$$\kappa = 0.508205 + (1.121081\varphi) + \left(0.057156 T^2\right) \quad (2)$$

The nanofluid heat capacity was then computed through the recommended expressions of Togun et al. [19] and Safaei et al. [7]:

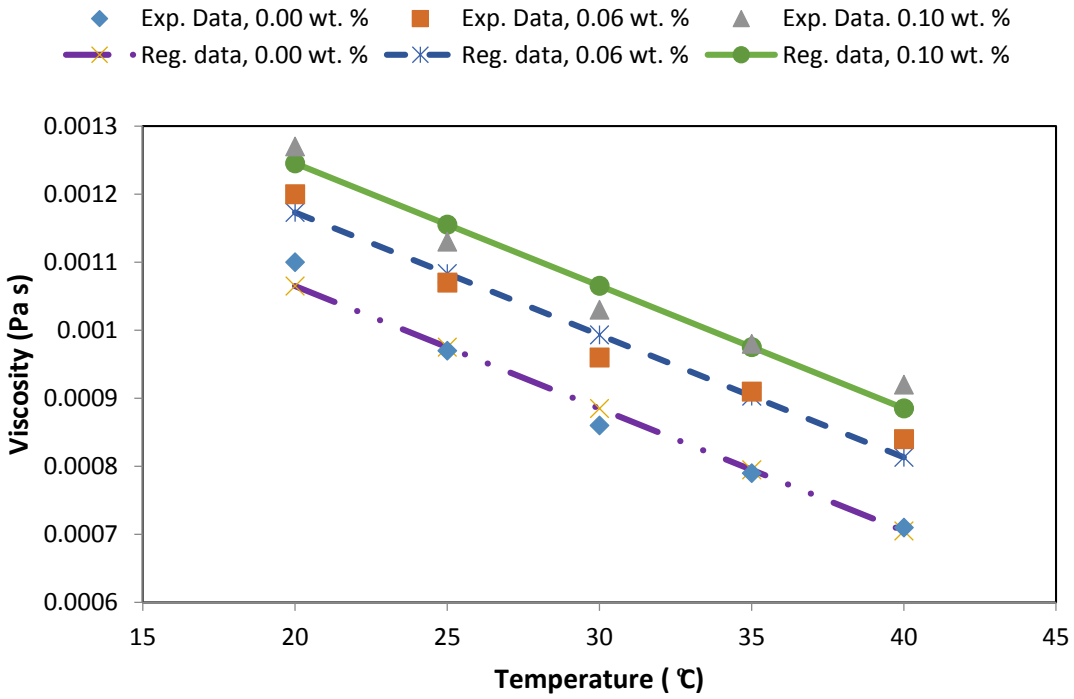
$$(\rho c_p)_{nf} = (1-\varphi)(\rho c_p)_f + \varphi(\rho c_p)_s \quad (3)$$

Figure 1 compares the predictions of Equations (1) and (2) for effective thermal conductivity and effective viscosity of the nanofluids for a range of temperature and solid fractions. It is seen that the effective thermal conductivity of nanofluids increases with the increase of temperature as well as the solid weight fraction. The net increase is about 30% for the range of parameters considered in this figure. Figure 1b shows that the effective viscosity of nanofluids increases with the increase of the solid weight fraction by about 8%, while the viscosity decreases sharply with the increase in temperature. The net decrease is about 45% in the range of the weight fraction and temperature considered.




(a)

**Figure 1.** *Cont.*




(**b**)

**Figure 1.** Comparison of the predictions of empirical Equations (1) and (2) with the experimental data. (**a**) Thermal conductivity; (**b**) Viscosity.

## 3. Physical Model

A rectangular duct with length $L$ = 2000 mm, width $W$ = 200 mm and depth $H$ = 25 mm was considered in this study. The outer surfaces of the duct heat exchanger are assumed to be insulated. The working nanofluids are mixture of water with GNP-silver. A range of solid volume fraction up to 0.1 wt. % was studied. The thermo-physical properties of the base fluid and nanosheets are provided in Table 1.

## 4. Empirical Expressions

In this simulation effort, fully developed flows in the turbulent regime are assumed [18,20]. The nanofluid is also incompressible. For the rectangular duct with width $W$ and height $H$, the cross-sectional area and wetted perimeter are given as:

$$A = WH \tag{4}$$

$$P = \sum_{i=0}^{\infty} l_i = 2(H + W) \tag{5}$$

The corresponding hydraulic diameter then becomes,

$$D_h = \frac{4A}{P} = \frac{2WH}{H + W} \tag{6}$$

The flow Reynolds number and the Peclet number are defined as:

$$\begin{aligned} \mathrm{Re} &= \frac{VD_h}{\upsilon_m} \\ Pe = \mathrm{RePr} &= \frac{VD_h}{\alpha_m} \end{aligned} \tag{7}$$

where $\mathrm{Pr} = \frac{\upsilon_m}{\alpha_m}$ is the Prandtl number where the heat diffusivity of the nanofluid is given as

$$\alpha_m = \frac{k_m}{\rho_m C_p} \tag{8}$$

and

$$\upsilon_m = \frac{\mu_m}{\rho_m} \tag{9}$$

is the kinematic viscosity of the nanofluid.

The Nusselt number in fully developed duct flows in a turbulent flow regime is given as [18]:

$$Nu = \frac{hD_h}{k} = 0.0017066\mathrm{Pr}^{1.29001}\mathrm{Re}^{0.9253} \tag{10}$$

Following the work of Yarmand et al. [18], the friction factor is estimated as:

$$f = 0.567322\phi^{0.0271605}\mathrm{Re}^{-0.285869} \tag{11}$$

The pressure drop and pumping power of the nanofluid are given, respectively, as:

$$\Delta p = f\left[\frac{L\rho_m V^2}{2D_h}\right] \tag{12}$$

$$P_p = VA\Delta p \tag{13}$$

The predictions of Equations (10)–(12) were evaluated compared with the CFD results and the experimental data for model validation in the following section.

## 5. Governing Equations for CFD Simulation

Based on the recommendation of [21,22], for the CFD modeling of nanofluids, the equations of continuity, momentum, energy and transport for k and $\varepsilon$ according to the Renormalization Group (RNG) turbulence model are solved. These are:

$$\frac{\partial u}{\partial x} + \frac{\partial v}{\partial y} = 0 \tag{14}$$

$$u\frac{\partial u}{\partial x} + v\frac{\partial u}{\partial y} = -\frac{1}{\rho}\frac{\partial p}{\partial x} + \frac{\partial}{\partial x}[(\upsilon_m + \upsilon_t)(2\frac{\partial u}{\partial x})] + \frac{\partial}{\partial y}[(\upsilon_m + \upsilon_t)(\frac{\partial u}{\partial y} + \frac{\partial v}{\partial x})] \tag{15}$$

$$u\frac{\partial v}{\partial x} + v\frac{\partial v}{\partial y} = -\frac{1}{\rho}\frac{\partial p}{\partial y} + g\beta(T - T_m) + \frac{\partial}{\partial y}[(\upsilon_m + \upsilon_t)(2\frac{\partial v}{\partial y})] + \frac{\partial}{\partial x}[(\upsilon_m + \upsilon_t)(\frac{\partial v}{\partial x} + \frac{\partial u}{\partial y})] \tag{16}$$

$$u\frac{\partial T}{\partial x} + v\frac{\partial T}{\partial y} = \frac{\partial}{\partial x}[(\alpha_m + \frac{\upsilon_t}{\sigma_T})\frac{\partial T}{\partial x}] + \frac{\partial}{\partial y}[(\alpha_m + \frac{\upsilon_t}{\sigma_T})\frac{\partial T}{\partial y}] \tag{17}$$

$$u\frac{\partial k}{\partial x} + v\frac{\partial k}{\partial y} = \frac{\partial}{\partial x}[(\upsilon_m + \frac{\upsilon_t}{\sigma_k})\frac{\partial k}{\partial x}] + \frac{\partial}{\partial y}[(\upsilon_m + \frac{\upsilon_t}{\sigma_k})\frac{\partial k}{\partial y}] + P_k + G_k - \varepsilon \tag{18}$$

$$u\frac{\partial \varepsilon}{\partial x} + v\frac{\partial \varepsilon}{\partial y} = \frac{\partial}{\partial x}[(\upsilon_m + \frac{\upsilon_t}{\sigma_\varepsilon})\frac{\partial \varepsilon}{\partial x}] + \frac{\partial}{\partial y}[(\upsilon_m + \frac{\upsilon_t}{\sigma_\varepsilon})\frac{\partial \varepsilon}{\partial y}] + C_1\frac{\varepsilon}{k}P_k + C_2\frac{\varepsilon^2}{k} + C_3\frac{\varepsilon}{k}G_k - R_\varepsilon \tag{19}$$

Here $\alpha_m$ and $\upsilon_m$ are given by Equations (8) and (9) and the effective viscosity and heat conductivity are given by Equations (1) and (2).

The eddy viscosity is evaluated from the Prandtl-Kolmogorov relation:

$$\upsilon_t = C_\mu f_\mu \frac{k^2}{\varepsilon} \tag{20}$$

The turbulence kinetic energy production term is given as:

$$P_k = v_t \left[ 2\left(\frac{\partial u}{\partial x}\right)^2 + 2\left(\frac{\partial v}{\partial x}\right)^2 + \left(\frac{\partial u}{\partial y} + \frac{\partial v}{\partial y}\right)^2 \right] \tag{21}$$

The buoyancy term, $G_k$, is obtained from:

$$G_k = -g\beta \frac{v_t}{\sigma_t} \frac{\partial T}{\partial y} \tag{22}$$

Also, $R_\varepsilon$ in the $\varepsilon$ equation is calculated through the following expressions:

$$R_\varepsilon = \frac{C_\mu \rho \eta^3 \left(1 - \frac{\eta}{\eta_0}\right)}{1 + \beta \eta^3} \frac{\varepsilon^2}{k} \tag{23}$$

$$\eta = \frac{Sk}{\varepsilon} \tag{24}$$

The constants of Equations (18) to (24) can be found in Table 2.

**Table 2.** Coefficients for RNG k-ε turbulence model [23,24].

| $C_\mu$ | $\sigma_k$ | $\sigma_\varepsilon$ | $C_1$ | $C_2$ | $\eta_0$ | β | K |
|---|---|---|---|---|---|---|---|
| 0.0845 | 1 | 1.3 | 1.42 | 1.68 | 4.38 | 0.012 | 0.41 |

## 6. Validation

*Validation of Heat Transfer for Graphene Nanoplatelets–Silver/Wate Nanofluids*

To validate the present model for turbulent-forced convection of GNP-silver nanofluids, the predictions of Equations (10) and (11) are compared with the experimental data and the CFD results obtained with use of the ANSYS-FLUENT commercial software. In their study, Yarmand et al. [18] experimentally measured the thermo-physical properties of distilled water/GNP-silver nanofluids as well as the corresponding friction factor and Nusselt number during the flow in a horizontal stainless steel tube under uniform heat flux. The experimental test section had a 10 mm inner diameter, a 12.8 mm outer diameter, and a length of 1.4 m. Experiments were performed in the range of $5000 \leqslant Re \leqslant 17{,}500$, which in the turbulent flow regime. The CFD model was performed using the single-phase fluid model with the effective viscosity and thermal conductivity given by Equations (1) and (2) using the ANSYS-FLUENT code [21,22].

For a nanofluid with 0.10 wt. % GNP-silver, the predicted variations of the friction factor as well as the Nusselt number for a range of Reynolds numbers are compared with the experimental data of Yarmand et al. [18] and the results of the CFD study in Figure 2a,b. It is seen that the present model predictions are in good agreement with the experimental data. However, the CFD simulation results slightly over the predictions of the experimental data. This is attributed to the neglecting effect of the tube outer diameter in the CFD simulations. Overall, from Figure 2, it is inferred that the present modeling approach is suitable for evaluating the friction factor for the flow of graphene nanoplatelets–silver/water nanofluids.

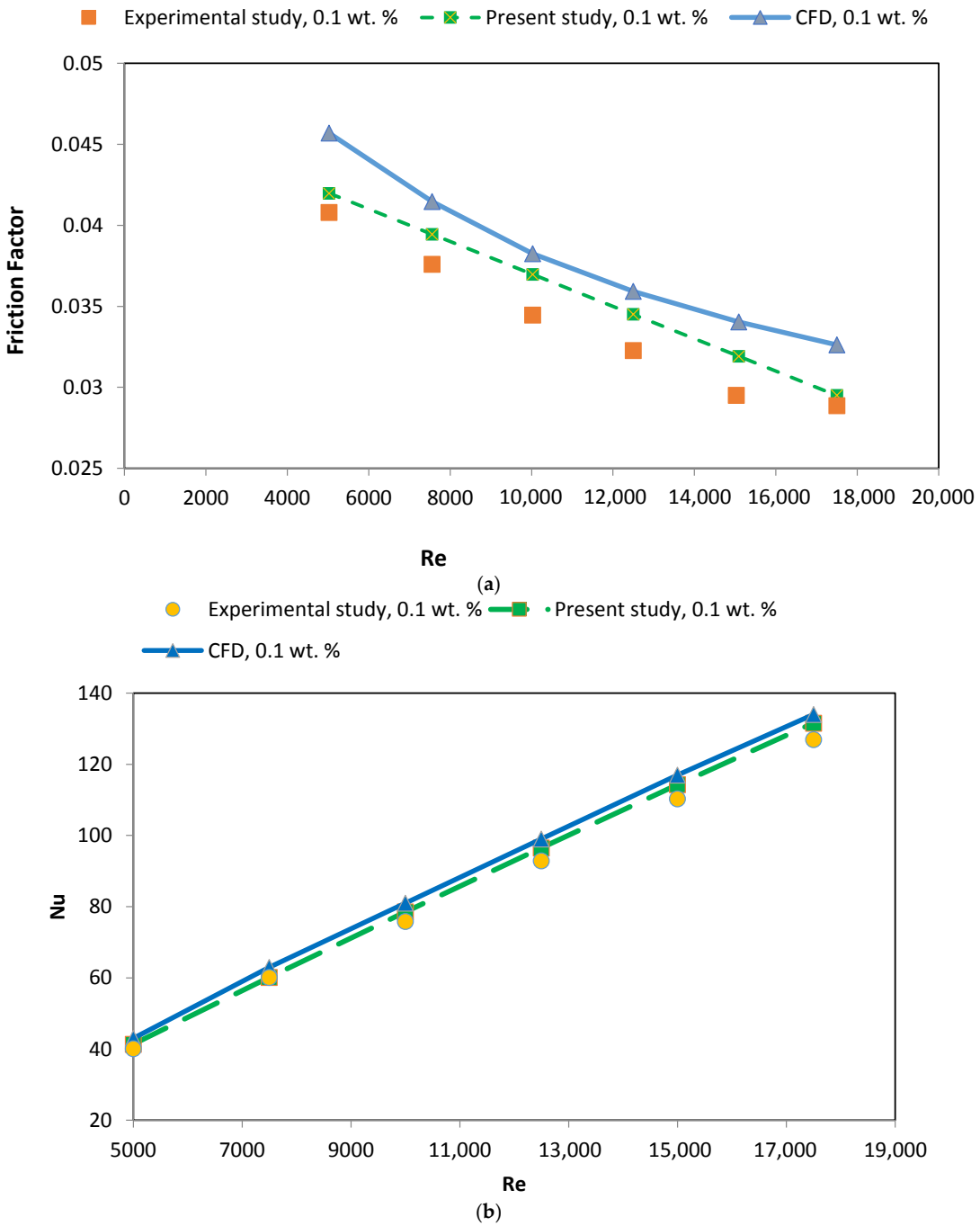



**Figure 2.** Comparison of the predicted friction factor and Nusselt number for ϕ = 0.10 wt. % with the experimental data of [18] and the CFD results. (**a**) Friction factor; (**b**) Nusselt number.

## 7. Results and Discussion

Figure 3 shows the variation of the Nusselt number with the Reynolds number for water and nanofluids with various solid weight percentages. It is seen from the figure that the value of the Nusselt number for the base fluid is lower than those of the nanofluids. Also the Nusselt number increases as the flow Reynolds number increases and/or when the concentration of nanosheets increases. The increase of the *Nu* with *Re*, which also occurs for the base fluid, is due to the increase of flow velocity and the associated transport processes in turbulent flows.

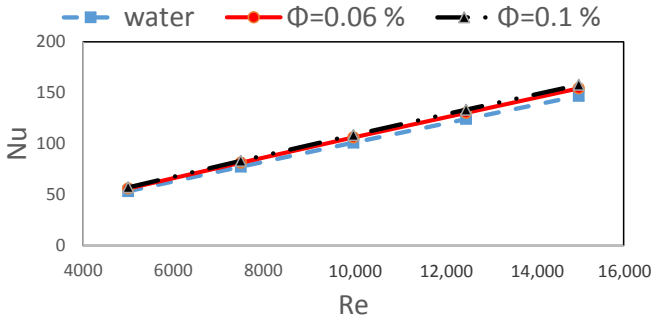



**Figure 3.** Variation of Nusselt number versus Reynolds numbers for different weight percentages of nanosheets.

The higher heat transfer for nanofluids compared to the distillated water is due to the following mechanisms:

(1) The Brownian motion of nanosheets and the associated micro-scale fluid motion.
(2) An increase in the overall thermal conductivity of the suspension as a result of the high thermal conductivity of nanosheets suspended in the carrying fluid.
(3) A rise in the effective heat transfer surface area among the dispersed nanosheets and the base fluid [16].

In addition, it should be pointed out that the viscosity of the nanofluid increases due to the increase in the nanosheet concentration. Thus, for a fixed pressure drop, a decrease in the Reynolds number and, as a result, a reduction in Nusselt number is anticipated. In summary, Figure 3 points out a direct relationship between the Nusselt number and the concentration of nanosheets, demonstrating the recognizable influence of thermal conductivity on the convective heat transfer over a range of Reynolds numbers.

Figure 4 shows the variation of the friction factor with the Reynolds number for different nanosheet weight percentages. The friction factor was calculated from the expression suggested by Yarmand et al. [18] and is given by Equation (11). Accordingly, the friction factor is a function of the Reynolds number as well as the nanosheet weight percentage. Figure 4 shows that the friction factor decreases with the increase in the Reynolds number or with the reduction of the nanosheet concentration in the base fluid. These trends are similar to those reported by Ray et al. [25] and Goodarzi et al. [16].

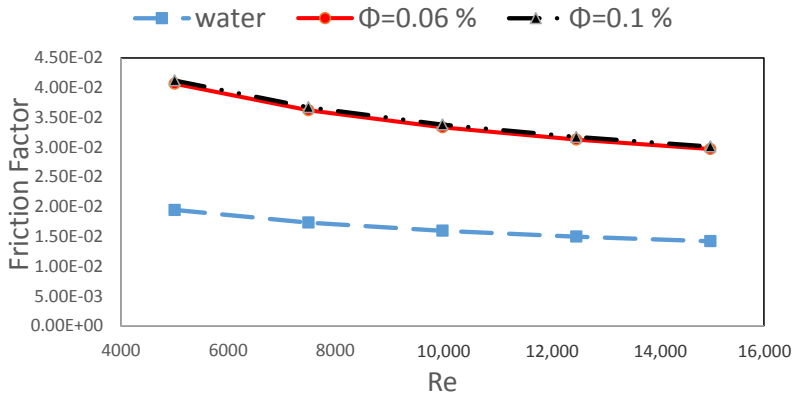



**Figure 4.** Variation of friction factor with Reynolds number for different nanosheet weight percentages.

In addition to the Nusselt number (heat transfer coefficient), another significant parameter to consider for practical applications of nanofluids in the industry is the flow pressure drop. The variations

of pressure drop with the Reynolds number for various solid weight percentages are shown in Figure 5. The pressure drop is a function of the inlet velocity, the thermo-physical characteristics of the fluid and the ratio of the closed conduit length to its hydraulic diameter. Figure 5 shows that the pressure drop increases sharply with the Reynolds number. Moreover, for a particular Reynolds number, the pressure drop is the lowest point for water. The pressure drop increases with the nanosheet weight percentage and reaches its highest value at 0.1 wt. %, which is the highest solid concentration studied. Thus, with the increase in the dispersed nanosheets in the base fluid, both the density and viscosity of the nanofluid increase, causing a higher pressure drop.

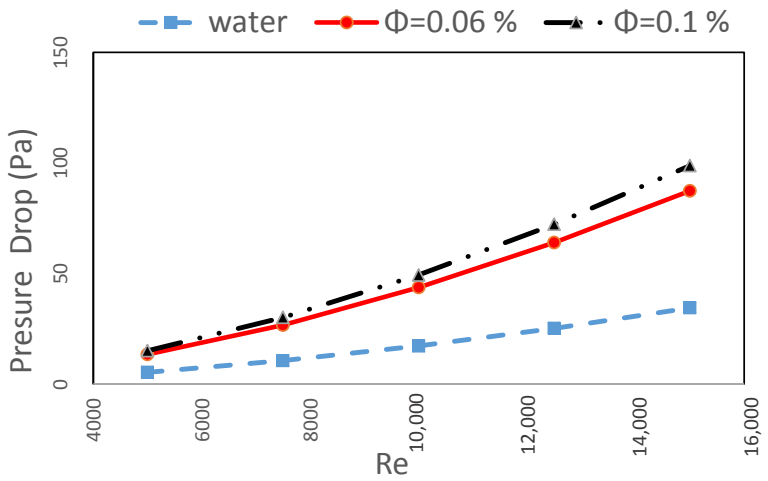



**Figure 5.** Variations of pressure drop with Reynolds number for different nanosheet weight percentages.

Pumping power is related to the pressure drop, flow rate and geometry of the closed conduit. Figure 6 shows the variation of pumping power versus Reynolds number. It is seen that the pumping power increases rapidly with *Re*. Similar to the pressure drop, the pumping power is the lowest for water, and increases with the nanosheet weight percentage, reaching its maximum values for 0.01 wt. %.

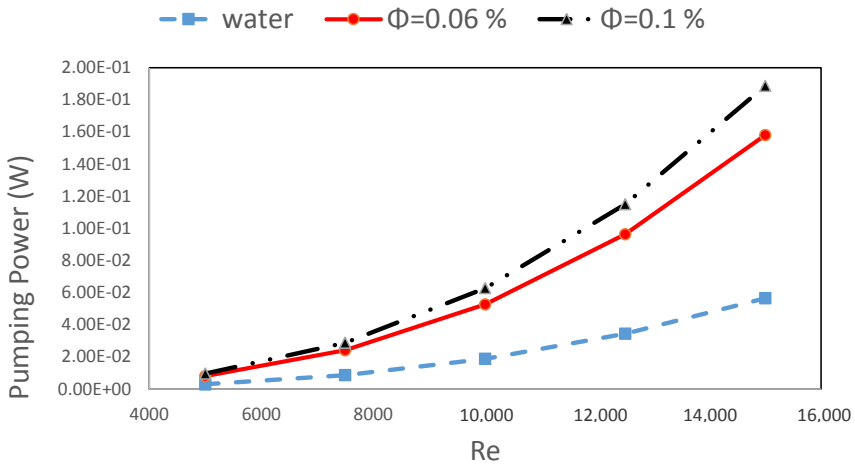



**Figure 6.** Variation of pumping power versus Reynolds number for different nanosheet weight percentages.

## 8. Conclusions

In this study, the performance of GNP-silver water-based nanofluids at different weight percentages flowing in a rectangular duct was tested. A range of turbulent flows with different

Reynolds numbers were considered. The enhancement in heat transfer as well as the required pumping power were evaluated and were reported for a cost-benefit analysis of using the GNP-silver nanofluid for practical applications.

The presented results suggest that using a proper concentration of nanosheets in the nanofluid led to an enhancement in the heat transfer compared with the base fluid. In addition, it was shown that the increase in the nanosheet weight percentage increased the friction factor, as well as the corresponding pressure drop and pumping power.

It was concluded that the GNP-silver water-based nanofluid could be used as an effective working fluid in increasing the efficiency of heat transfer in heat exchangers.

**Acknowledgments:** The authors gratefully acknowledge High Impact Research Grant UM.C/HIR/MOHE/ENG/23 and Faculty of Engineering, University of Malaya, Malaysia for support in conducting this research work.

**Author Contributions:** The numerical part and coding has been done by Mohammad Reza Safaei and Mohammad Shahab Goodarzi. The manuscript has been written through the contributions of Goodarz Ahmadi, Mostafa Safdari Shadloo, Hamid Reza Goshayeshi and Mahidzal Dahari. All authors read and approved the final manuscript.

**Conflicts of Interest:** The authors declare no conflict of interest. The founding sponsors had no role in the design of the study; in the collection, analyses, or interpretation of data; in the writing of the manuscript, and in the decision to publish the results.

## Nomenclature

| | |
|---|---|
| $A$ | Area (m) |
| $H$ | Depth of the channel (m) |
| $f$ | Friction factor |
| $h$ | Heat transfer coefficient ($\mathrm{W}\cdot\mathrm{m}^{-2}\cdot\mathrm{K}^{-1}$) |
| $D_{\mathrm{h}}$ | Hydraulic diameter (m) |
| $l$ | Length of each surface in contact with the aqueous body (m) |
| $L$ | Length of the channel (m) |
| $Nu$ | Nusselt number |
| $Pr$ | Prandtl number |
| $Pe$ | Peclet number |
| $p$ | Pressure (Pa) |
| $P_p$ | Pumping power (W) |
| $Re$ | Reynolds number |
| $C_p$ | Specific heat capacity ($\mathrm{J}\cdot\mathrm{kg}^{-1}\cdot\mathrm{K}^{-1}$) |
| $T$ | Temperature (K) |
| $\kappa$ | Thermal conductivity ($\mathrm{W}\cdot\mathrm{m}^{-1}\cdot\mathrm{K}^{-1}$) turbulence |
| $V$ | Velocity ($\mathrm{m}\cdot\mathrm{s}^{-1}$) |
| $u$ | Velocity, $x$-component ($\mathrm{m}\cdot\mathrm{s}^{-1}$) |
| $v$ | Velocity, $y$-component ($\mathrm{m}\cdot\mathrm{s}^{-1}$) |
| $P$ | Wetted perimeter (m) |
| $W$ | Width of the channel (m) |

## Greek Symbols

| | |
|---|---|
| $\rho$ | Density ($\mathrm{kg}\cdot\mathrm{m}^{-3}$) |
| $\mu$ | Dynamic viscosity ($\mathrm{Pa}\cdot\mathrm{s}$) |
| $\upsilon$ | Kinematics viscosity ($\mathrm{m}^2\cdot\mathrm{s}^{-1}$) |
| $\alpha$ | Thermal diffusivity ($\mathrm{m}^2\cdot\mathrm{s}^{-1}$) |
| $\kappa$ | Thermal conductivity ($\mathrm{m}^2\cdot\mathrm{s}^{-2}$) |

| | |
|---|---|
| $\varepsilon$ | Turbulence dissipation ($m^2 \cdot s^{-3}$) |
| $\eta$ | Thermal performance factor |
| $\varphi$ | Weight percentage of nanosheets |

### Subscripts

| | |
|---|---|
| *bf* | Base fluid |
| *m* | Mixture |
| *i* | Indices |
| *t* | Turbulence |

## References


1. Huminic, G.; Huminic, A. Application of nanofluids in heat exchangers: a review. *Renew. Sustain. Energy Rev. 16*, 5625–5638. [CrossRef]
2. Mehrizi, A.A.; Farhadi, M.; Sedighi, K.; Delavar, M.A. Effect of fin position and porosity on heat transfer improvement in a plate porous media heat exchanger. *J. Taiwan Inst. Chem. Eng.* **2013**, *44*, 420–431. [CrossRef]
3. Gut, J.A.W.; Fernandes, R.; Pinto, J.M.; Tadini, C.C. Thermal model validation of plate heat exchangers with generalized configurations. *Chem. Eng. Sci.* **2004**, *59*, 4591–4600. [CrossRef]
4. Dwivedi, A.K.; Das, S.K. Dynamics of plate heat exchangers subject to flow variations. *Int. Heat Mass Transf.* **2007**, *50*, 2733–2743. [CrossRef]
5. Choi, S.U.; Eastman, J. *Enhancing Thermal Conductivity of Fluids with Nanoparticles*; Argonne National Lab.: Lemont, IL, USA, 1995.
6. Safaei, M.; Mahian, O.; Garoosi, F.; Hooman, K.; Karimipour, A.; Kazi, S.; Gharehkhani, S. Investigation of micro-and nanosized particle erosion in a 90° pipe bend using a two-phase discrete phase model. *Sci. World J.* **2014**, *2014*, 740578. [CrossRef] [PubMed]
7. Safaei, M.R.; Togun, H.; Vafai, K.; Kazi, S.N.; Badarudin, A. Investigation of Heat Transfer Enhancement in a Forward-Facing contracting Channel using FMWCNT Nanofluids. *Numer. Heat Transf.* **2014**, *66*, 1321–1340. [CrossRef]
8. Goodarzi, M.; Safaei, M.R.; Vafai, K.; Ahmadi, G.; Dahari, M.; Kazi, S.N.; Jomhari, N. Investigation of nanofluid mixed convection in a shallow cavity using a two-phase mixture model. *Int. J. Therm. Sci.* **2014**, *75*, 204–220. [CrossRef]
9. Wu, J.M.; Zhao, J. A review of nanofluid heat transfer and critical heat flux enhancement—Research gap to engineering application. *Prog. Nucl. Energy* **2013**, *66*, 13–24. [CrossRef]
10. Sonawane, S.S.; Khedkar, R.S.; Wasewar, K.L. Study on concentric tube heat exchanger heat transfer performance using $Al_2O_3$-water based nanofluids. *Int. Commun. Heat Mass Transf.* **2013**, *49*, 60–68. [CrossRef]
11. Pandey, S.D.; Nema, V.K. Experimental analysis of heat transfer and friction factor of nanofluid as a coolant in a corrugated plate heat exchanger. *Exp. Therm. Fluid Sci.* **2012**, *38*, 248–256. [CrossRef]
12. Taws, M.; Nguyen, C.T.; Galanis, N.; Gherasim, I. Experimental Investigation of Nanofluid Heat Transfer in a Plate Heat Exchanger, Proceedings of the ASME 2012 Heat Transfer Summer Conference Collocated with the ASME 2012 Fluids Engineering Division Summer Meeting and the ASME 2012 10th International Conference on Nanochannels, Microchannels, and Minichannels, Rio Grande, Puerto Rico, 8–12 July 2012; American Society of Mechanical Engineers: New York, NY, USA, 2012; pp. 1–8.
13. Elias, M.M.; Saidur, R.; Rahim, N.A.; Sohel, M.R.; Mahbubul, I.M. Performance Investigation of a Plate Heat Exchanger Using Nanofluid with Different Chevron Angle. *Adv. Mater. Res.* **2014**, *832*, 254–259. [CrossRef]
14. Sarafraz, M.M.; Hormozi, F. Heat transfer, pressure drop and fouling studies of multi-walled carbon nanotube nano-fluids inside a plate heat exchanger. *Exp. Therm. Fluid Sci.* **2016**, *72*, 1–11. [CrossRef]
15. Goodarzi, M.; Kherbeet, A.S.; Afrand, M.; Sadeghinezhad, E.; Mehrali, M.; Zahedi, P.; Wongwises, S.; Dahari, M. Investigation of heat transfer performance and friction factor of a counter-flow double-pipe heat exchanger using nitrogen-doped, graphene-based nanofluids. *Int. Commun. Heat Mass Transf.* **2016**, *76*, 16–23. [CrossRef]

16. Goodarzi, M.; Amiri, A.; Goodarzi, M.S.; Safaei, M.R.; Karimipour, A.; Languri, E.M.; Dahari, M. Investigation of heat transfer and pressure drop of a counter flow corrugated plate heat exchanger using MWCNT based nanofluids. *Int. Commun. Heat Mass Transf.* **2015**, *66*, 172–179. [CrossRef]
17. Hassan, M.; Sadri, R.; Ahmadi, G.; Dahari, M.B.; Kazi, S.N.; Safaei, M.R.; Sadeghinezhad, E. Numerical study of entropy generation in a flowing nanofluid used in micro-and minichannels. *Entropy* **2013**, *15*, 144–155. [CrossRef]
18. Yarmand, H.; Gharehkhani, S.; Ahmadi, G.; Shirazi, S.F.S.; Baradaran, S.; Montazer, E.; Zubir, M.N.M.; Alehashem, M.S.; Kazi, S.N.; Dahari, M. Graphene nanoplatelets-silver hybrid nanofluids for enhanced heat transfer. *Energy Convers. Manag.* **2015**, *100*, 419–428. [CrossRef]
19. Togun, H.; Ahmadi, G.; Abdulrazzaq, T.; Shkarah, A.J.; Kazi, S.; Badarudin, A.; Safaei, M.R. Thermal performance of nanofluid in ducts with double forward-facing steps. *J. Taiwan Inst. Chem. Eng.* **2015**, *47*, 28–42. [CrossRef]
20. Sadeghinezhad, E.; Mehrali, M.; Tahan Latibari, S.; Mehrali, M.; Kazi, S.N.; Oon, C.S.; Metselaar, H.S.C. Experimental investigation of convective heat transfer using graphene nanoplatelet based nanofluids under turbulent flow conditions. *Ind. Eng. Chem. Res.* **2014**, *53*, 12455–12465. [CrossRef]
21. Yarmand, H.; Ahmadi, G.; Gharehkhani, S.; Kazi, S.N.; Safaei, M.R.; Sadat Alehashem, M.; Mahat, A.B. Entropy generation during turbulent flow of zirconia-water and other nanofluids in a square cross section tube with a constant heat flux. *Entropy* **2014**, *16*, 6116–6132. [CrossRef]
22. Yarmand, H.; Gharehkhani, S.; Kazi, S.N.; Sadeghinezhad, E.; Safaei, M.R. Numerical investigation of heat transfer enhancement in a rectangular heated pipe for turbulent nanofluid. *Sci. World J.* **2014**, *2014*, 1–9. [CrossRef] [PubMed]
23. Safaei, M.R.; Goshayshi, H.R.; Saeedi Razavi, B.; Goodarzi, M. Numerical investigation of laminar and turbulent mixed convection in a shallow water-filled enclosure by various turbulence methods. *Sci. Res. Essays* **2011**, *6*, 4826–4838.
24. Safaei, M.R.; Goodarzi, M.; Mohammadi, M. Numerical modeling of turbulence mixed convection heat transfer in air filled enclosures by finite volume method. *Int. J. Multiphys.* **2011**, *5*, 307–324. [CrossRef]
25. Ray, D.R.; Das, D.K.; Vajjha, R.S. Experimental and numerical investigations of nanofluids performance in a compact minichannel plate heat exchanger. *Int. J. Hea Mass Transf.* **2014**, *71*, 732–746. [CrossRef]



© 2016 by the authors; licensee MDPI, Basel, Switzerland. This article is an open access article distributed under the terms and conditions of the Creative Commons Attribution (CC-BY) license (http://creativecommons.org/licenses/by/4.0/).